Available online at www.sciencedirect.com

ScienceDirect

journal homepage: www.elsevier.com/locate/he

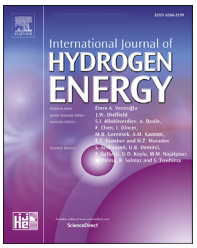

Design a promising electro-catalyst for oxygen reduction reaction in fuel cells based on transition metal doped in BN monolayer

Chou-Yi Hsu [a], *Nestor Ulloa* [b,*], *Eugenia Mercedes Naranjo Vargas* [b], *Shelesh Krishna Saraswat* [c,**], *Shakir Mahmood Saeed* [d], *S. Kevin Vargas-Portugal* [e], *Hasan Sh. Majdi* [f], *Abdelmajeed Adam Lagum* [g]

[a] *Department of pharmacy, Chia Nan University of Pharmacy and Science, Tainan, Taiwan*
[b] *Facultad de Ingeniería Mecánica, Escuela Superior Politécnica de Chimborazo (ESPOCH), Riobamba, 060155, Ecuador*
[c] *Department of Electronics and communication Engineering, GLA University, 281406, Mathura, Uttar Pradesh, India*
[d] *Department of Pharmacy, Al-Noor University College, Nineveh, Iraq*
[e] *Universidad Tecnológica de los Andes, Perú*
[f] *Department of Chemical Engineering and Petroleum Industries, Al- Mustaqbal University, 51001, Hilla, Iraq*
[g] *Department of Civil Engineering, Faculty of Engineering, Isra University, P.O. Box 22, Amman, 11622, Jordan*

HIGHLIGHTS

- The catalytic activity of a series of Co-doped v-BN has been theoretically explored in the ORR.
- O_2 molecule can be directly dissociated on the Co-doped v-BN with 4e pathway.
- It is reacting more favorable for the ER mechanism of OH* to convert into H_2O.
- The ORR reaction was found to be thermodynamically favorable in the Co-doped v-BN.

ARTICLE INFO

Article history:
Received 24 July 2023
Accepted 7 August 2023
Available online xxx

Keywords:
Oxygen reduction reaction
Fuel cells
Electrocatalyst
Adsorption energies
Thermodynamic driving force

ABSTRACT

The kinetic of the oxygen reduction reaction (ORR) at the cathodes of polymer-electrolyte-membrane fuel cells (PEMFCs) has been demonstrated to be slow, which is one of the pivotal issues in developing PEMFCs. Within the current piece of research, by performing first-principles calculations, we introduce a Co-doped vacancy BN nanosheet (Co-HBN) as an efficacious noble metal-free electro-catalyst for the ORR process (ORRP) in fuel cells. The results demonstrate a rise in the energies of adsorption (or adhesion) onto the Co−N active site of these electrocatalysts in the order of O < OH < OOH < O_2 < H_2O_2 < H_2O on this electrocatalyst and there is a consistent change in the adsorption energies (E_{ads})for all oxygen-containing intermediates (OCIs). Based on the small and large thermodynamic driving force for the generation of H_2O_2 and for reducing OOH into O* (or to 2OH*), respectively, the four-electron route was more favorable in comparison with the $2e^-$ route. Furthermore, with the largest value of ΔG for Co-HBN electrocatalyst, the final reduction step ($OH^* + H^+ + e^- \rightarrow H_2O + *$) has been regarded as the rate-limiting step. The d-band center of Co was considerably distant from the Fermi level. The greater gap between the

* *Corresponding author.*
** *Corresponding author.*
E-mail addresses: nestor.ulloa@espoch.edu.ec (N. Ulloa), sheleshkrishnasaraswat@gmail.com (S.K. Saraswat).
https://doi.org/10.1016/j.ijhydene.2023.08.085

frontier orbitals suggested that the electrocatalyst is not conducive to the adsorption of OCIs, which shows that the onset potential is larger and ORR is high.

1. Introduction

The problems of environmental pollution and energy crisis in the world can be resolved by using renewable and clean energy systems. Polymer-electrolyte-membrane fuel cells (PEMFCs) are promising and efficacious renewable energy systems in terms of energy and they have negligible exhaust emissions and high energy density [1–5]. Moreover, at a lower temperature, PEMFCs have high operating efficiency. Nonetheless, the kinetic of the oxygen reduction reaction (ORR) at the cathodes in PEMFCs has been revealed to be slow, which appreciably reduces the fuel cells' performance [6–9]. These days, Pt/C is widely employed as a cathode fuel cell electrocatalysts. Nevertheless, the extensive use of platinum in automobiles is limited by its poor durability, scarcity, and high price. Hence, sustainable and cheap ORR electrocatalysts such as catalysts based on non-precious metals are considered to be best alternative [10].

In the last decades, several research groups have investigated the potential of transition metal oxides [11] or carbon materials doped with heteroatoms [12–14] for ORR. Co-doped graphene (Gr) catalysts using non-noble metals, including N, Mn, Fe and Co are promising options for Pt-based catalysts because of their cheapness and higher activity [15,16]. Because of their great activity and durability for ORR in acidic as well as alkaline environments, N and Co codoped Gr catalysts have aroused considerable interest among the M-N-C catalysts which are presently developed. For instance, in a piece of research by Jiang et al. [17], cobalt nitrate incorporated within polypyrrole/Gr oxide was employed and it was subjected to annealing for the preparation of CoN_x-Gra. It was found that similar to the ORR performance of Pt/C catalysts, the ORR performance of CoN_x-Gra and its methanol tolerance was great. In a piece of research by Niu et al. [13], a 2-stage heat treatment method was adopted for preparing N and Co co-doped Gr catalyst. The findings demonstrated that ORR proceeded through a four-electron process. In another study by Yin et al. [18], a novel method was developed to obtain Co single atoms with stability on porous carbon doped with N with metal loading of 4 wt%. They found that the ORR performance was great and the half wave potential was 0.881 V. Moreover, a novel 3D mesoporous Co–N–C nano-sheet was developed by Han et al. in which some Co nano-particle nanohybrids were encapsulated. The activity of such nanohybrids for ORR is more in comparison with pure Co–N–C [19].

Because of their outstanding performance in chemical processes like ORR in fuel cells, carbon nano-materials such as Gr are regarded as promising alternatives for metal-free electrocatalysts [20–23]. In addition to Gr-like materials, 2-D nano-structures like hexagonal boron nitride (HBN) have unique chemical and physical attributes for different applications [24–26].

In comparison with Gr, there are several merits to *HBN*, for example high resistance, improved conductance and thermal stability [27–29]. Additionally, the adhesion properties of ionic and gas molecules are promoted by the exceptional surface area as well as the ionic B–N bonds of *HBN* due to the induced dipole moment. The chemical and physical properties of *HBN* hare unique, which make *HBN* an encouraging candidate for application in various fields like cathode FCs, optics and hydrogen storages [30–33]. The authors suggest that the Co-doped of pure and defective HBN have outstanding activity due to their unique composition and structure. Nevertheless, researcher have not assessed doped and defective BN activity of ORR at the atomic level. The results demonstrated that activity of transition metal (TM)-N_x sites is superior, particularly that of sites TM-N_4. Moreover, the Co–N_4 center led to a thorough 4-electron reduction of O_2 into H_2O, whereas Co–N_2 center prompted H_2O_2 formation [34–36].

The structure of Co-doped HBN as well as its ORR mechanism still remains unclear. Here, we investigated the ORR stability and activity for Co–N active center (AC) following defecting around the ACs of Co–N. Based on the results, some of the Co-doped electrocatalysts improved four-electron ORR activity and stability, which depended upon their doping places. Additionally, Co-doping led to some uplift on the surface of HBN, thus on two sides of the similar active site it caused varying catalytic activities. Therefore, we introduced a viable structure for the Co-doped HBN to enhance ORR performance and demonstrated the mechanism of ORR at the atomic scale.

2. Computations

All the structural optimizations and electronic energy computations were undertaken through density functional theory (DFT) natural charges have been performed by GAMESS program [37]. In order to describe correlation effects and the electronic exchange, we employed the functional GGA as parameterized by B3LYP. The 6-31 + G (d,p) level of theory was applied here for optimizing using B3LYP. Also, we used dispersion corrections by Grimme's DFT-D3 [38] scheme which explains weak van der Waals interactions. The convergence standard for maximum displacement, for and energy, respectively, was considered to be 1.0×10^{-6} Ha, 0.003 Ha/Å and Å. In order to assess the stability of Co-embedded HBN structures, their formation energy was computed as follows:

$$E_{form} = E_{Co-doped\ h-BN} + \mu_N + \mu_B - (E_{h-BN} + \mu_{Co}) \quad (1)$$

where $E_{Co\text{-}doped\ HBN}$ signifies the total energy of Co-embedded HBN and E_{HBN} signifies that of perfect HBN. μ_B and μ_N, respectively, signify the B atom's chemical potential in the α-rhombohedral B crystal and that of the N atom in the N_2

Please cite this article as: Hsu C-Y et al., Design a promising electro-catalyst for oxygen reduction reaction in fuel cells based on transition metal doped in BN monolayer, International Journal of Hydrogen Energy, https://doi.org/10.1016/j.ijhydene.2023.08.085

molecule [39]. The results demonstrated the thermodynamic stability of these catalytic sheets. The Mulliken population analysis was carried out for computing the charge on each atom for the electrocatalyst structures under study. The adsorption energy (E_{ads}) of oxygen-containing intermediates (OCIs), namely O_2, OOH, O, OH, H_2O and H_2O_2, was estimated as follows:

$$E_{ads} = E_{Co-h-BN+species} - \left(E_{species} + E_{Co-h-BN+species}\right) \quad (2)$$

where $E_{Co\text{-}HBN,+species}$ $E_{Co\text{-}HBN}$ and $E_{species}$, respectively, signify the total energy of Co-HBN with adsorbed molecules, Co-HBN without adsorbate and with free adsorbate. In order to compute every elementary reaction's free energy change, which occurs on these electrocatalysts' active site, we used the method which was suggested by Norskov et al., [40]. We can express each reduction step as below:

$$\Delta G = \Delta E - T\Delta S + \Delta ZPE + \Delta G_{field} + \Delta G_U + \Delta G_{pH} \quad (3)$$

here, ΔE signifies reaction energy, T signifies the temperature (289.15 K), ΔS signifies the entropy variation. ΔZPE signifies the zero-point energies. Additionally, we can compute ΔS and ΔZPE based on the vibration frequency of OCIs. ΔG_{pH} signifies the free energy contribution thanks to the variations of pH and ΔG_U signifies the electrode potential U. $\Delta G_{pH} = k_B \times pH \times \ln 10$ can be used to express the impact of pH upon the Gibbs free energy, where k_B signifies the Boltzmann constant. Moreover, $\Delta G_U = -neU$ is used to express the impact of electric potential upon Gibbs free energy, where and U signifies the electrode potential and n signifies the number of transported electrons. Here, the environment of the ORR was assumed to be acidic, and its pH was considered to be 0. We can ignore the impact of ΔG_{field} within this work because of its negligible impact upon the results of computations [40]. Moreover, we set the reference electrode as a standard hydrogen electrode, and when the reaction was under standard conditions at 298.15 K with the pH of 0 and U of 0 V, the free energy of H^+ in the electrode solution corresponded to half of the free energy of H_2. We computed the free energy change for the overall reaction $O_2 + 2H_2 \rightarrow 2H_2O$ at a pressure of 0.035 bar at 298.15 K in the solvent phase, which was computed to be 4.92 eV.

3. Results and discussion

3.1. *Electronic attributes and stability of the Co-doped-HBN*

Fig. 1 (a) demonstrates the geometry of pristine h-B. After the geometric relaxation, it was found that the 6-ring structure in HBN was destroyed. Our The lattice parameter of HBN was 6.89 Å, which was similar to values reporter in the literature [41]. The pristine HBN had a band gap of approximately 5.64 eV, which was similar to thee values reported in the literature [42] and demonstrated reliability of approach adopted in the current research, so it was capable of providing an exact account of the electronic geometry of HBN. A single N (V_N) or B (V_B) vacancy in *HBN* had to be created first in order to create the Co-doped *HBN*. Fig. 1b illustrates the geometries vacancy defective of HBN with most stability. In both defects V_N and V_B, the BN nanosheet retained its planar structure. The findings demonstrated that, in comparison with a nitrogen vacancy, a boron vacancy in *HBN* is superior in terms of energy, which was due to the fact that the loose N atoms repelled each other that stops the formation of unstable N–N bonds. It is worth mentioning that there was no stable divacancy (V_{BN}) in the present study. However, several research studies [43] demonstrated the likelihood of the formation of such paired vacancy in *HBN*.

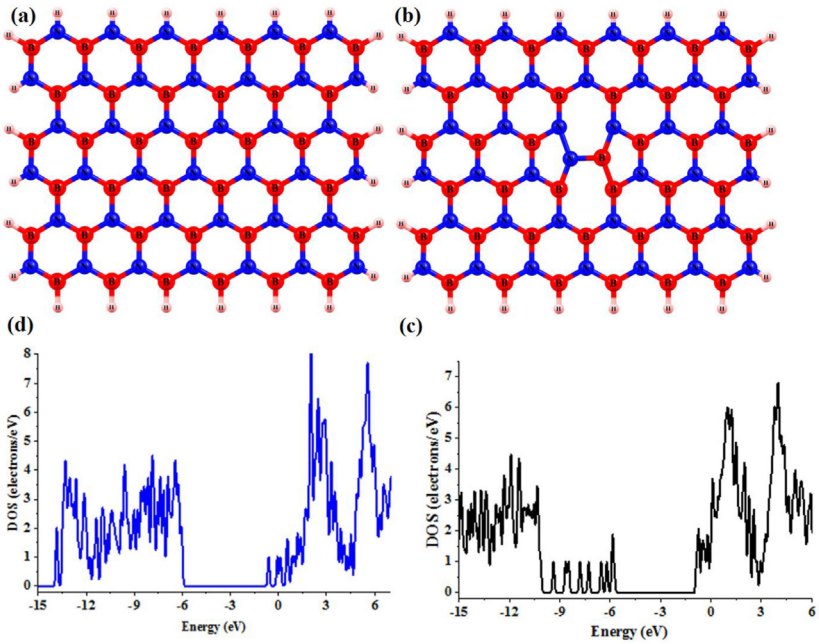

Fig. 1 – Optimized structure of (a) *HBN* and (b) vacancy-BN monolayers, density of state plot (DOS) of (c) *HBN* and (d) vacancy-BN monolayers.

Please cite this article as: Hsu C-Y et al., Design a promising electro-catalyst for oxygen reduction reaction in fuel cells based on transition metal doped in BN monolayer, International Journal of Hydrogen Energy, https://doi.org/10.1016/j.ijhydene.2023.08.085

Moreover, in the energy gap region with the band gap of 4.97 eV, a clear spin-splitting with distinct defect levels was observed based on the DOS analysis of the vacancy defects. In connection with V_B, a magnetic moment (MM) of around 3 μ_B is caused due to a B vacancy defect. Additionally, right after the formation of a B vacancy in *HBN*, 3 occupied states (2 spin-down and 1 spin-up) is formed above the FL, which can be observed in the related DOS plot in Fig. 1c and d. Such donor were are mainly composed of N-2p states, which are concentrated on the loose N atoms around the defect site.

The defect site of B or N can be occupied by a Co atom, leading to the formation of 3 chemical interactions with the neighboring B or N. On B and N, the average Co–N and Co–B binding distance was 1.83 and 1.94 Å, respectively. For both Co-doped surfaces, the MM of the entire system was 0, indicating the disappearance of dangling states because of the strong interaction between the vacancy site and the Co atom. Since the atomic radius of Co was greater than missing B or N, Co pushed outwards from the surface of HBN surface by approximately 1.43 Å. The binding strength between the surface of the defective HBN and the metal atom, which is one of the pivotal issues in developing SACs, was computed by the subtraction of the energy of separate Co as well as defective HBN sub-systems from that of Co-doped substrate for evaluating the stability of Co-doped *vacancy*-BN structures. The binding energy of Co on B and N was −6.86 and −5.29 eV, respectively, which was significantly higher than the cohesive energy of solid Co (4.39 eV). Moreover, the values were greater compared to the E_{bind} Co on defective *HBN* [44]. Therefore, Co interacted strongly with the surface to avoid the clustering of Co atoms. Additionally, in order to evaluate the feasibility of the formation of Co-doped HBN structures, their formation energy was considered under normal conditions. Furthermore, the energy of formation for the binding of the Co atom on the B and N was−0.29 and 1.33 eV, respectively. Hence, it can be suggested that Co was preferentially located on site B site in HBN rather than on site N (see Fig. 2).

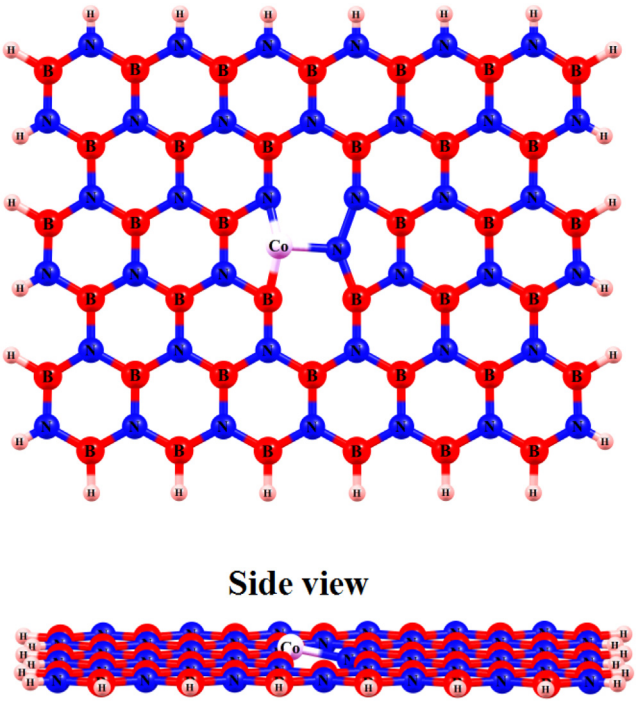

Fig. 2 – Optimized geometries of the Co-vacancy-BN monolayers (a) top and (b) side views.

3.2. *The adsorption energy of OCIs*

The adsorption attributes of ORR species, namely O_2, O, OH, OOH, H_2O and H_2O_2 on these electrocatalysts' surface were investigated. In all cases, several adhesion sites were considered, namely top of the Co, B, and N atoms, and over the B–N or Co-bonds. It was revealed that the easiest active site for the OCIs' adhesion was the Co atom' top site. Fig. 3 demonstrates the adsorption configurations of these electrocatalysts with most stability. For instance, the related E_{ads} and bond length of on this catalyst is provided in Table 1. Furthermore, the E_{ads} of these OCIs is demonstrated in Fig. 4. Based on the results, there was a reduction in the E_{ads} of these OCIs in the order of O > OH > OOH > O_2 > H_2O_2 > H_2O on this electrocatalyst. Additionally, there was consistent trend in the change in the E_{ads} for all OCIs, i.e., a higher E_{ads} of O_2 means that other OCIs also have stronger free E_{ads} at the same active site. Overall, O* preferred adhesion on the Co top site. Nevertheless, in connection with Co-doped HBN, O* was adsorbed over the bridge site (Co–N) rather than on the top site (Co), thus causing a higher E_{ads} of O*. However, it does not affect the onset potential. Before performing the first oxygen reduction step, the O_2 molecule adhesion on the Co top site with 2 configurations was a prerequisite. Based on the findings, the end-on structure was capable of being adsorbed onto the surface of these electrocatalysts in a more stable manner than the side-on structure. The onset potential value is usually determined by the OH adsorption strength usually determines. The weaker energy of OH adsorption was more helpful for the 4th ORR step. We observed that OH adsorbed onto the raised side of Co-doped HBN exhibited E_{ads} of −2.69 eV. After the co-adhesion of two paired OH onto the AC of Co–N, there was a reduction in the E_{ads} of each OH. For example, the average E_{ads} of each OH was −2.11 eV after the co-adsorption of two OH onto the surface of Co-doped HBN, which was weaker compared to the average E_{ads} of a single OH (0.58 eV). Clearly, a lower OH E_{ads} demonstrated that the reduction of OH was easier, demonstrating that the process of 2OH*(co-ad) $+H^+ + e^- \rightarrow OH^* + H_2O^*$ was easier to proceed in contrast to the process of $OH^* + H^+ + e^- \rightarrow H_2O^*$. Based on the computations, the first reaction had a much larger reaction free energy (RFE) than the second one on the active sites (see Table 2).

For the H_2O product, higher E_{ads} demonstrated that it was not capable of leaving the active site easily, which led to some freshly appeared ACs. The E_{ads} of H_2O on these electrocatalysts was small. This might one of the reasons for the promising nature of these electrocatalysts as ORR electrocatalysts. The bond distance of O–O for HOOH in the gaseous phase was 1.47 Å. After H_2O_2 was adsorbed onto the active site of these electrocatalysts, the length of O–Co was ~3.23 Å. There was no substantial rise in the bond distance of O–O (approximately 1.47 Å) in contrast to that of the H_2O_2 in the gaseous phase. The optimized geometry of H_2O_2 is optimized

Please cite this article as: Hsu C-Y et al., Design a promising electro-catalyst for oxygen reduction reaction in fuel cells based on transition metal doped in BN monolayer, International Journal of Hydrogen Energy, https://doi.org/10.1016/j.ijhydene.2023.08.085

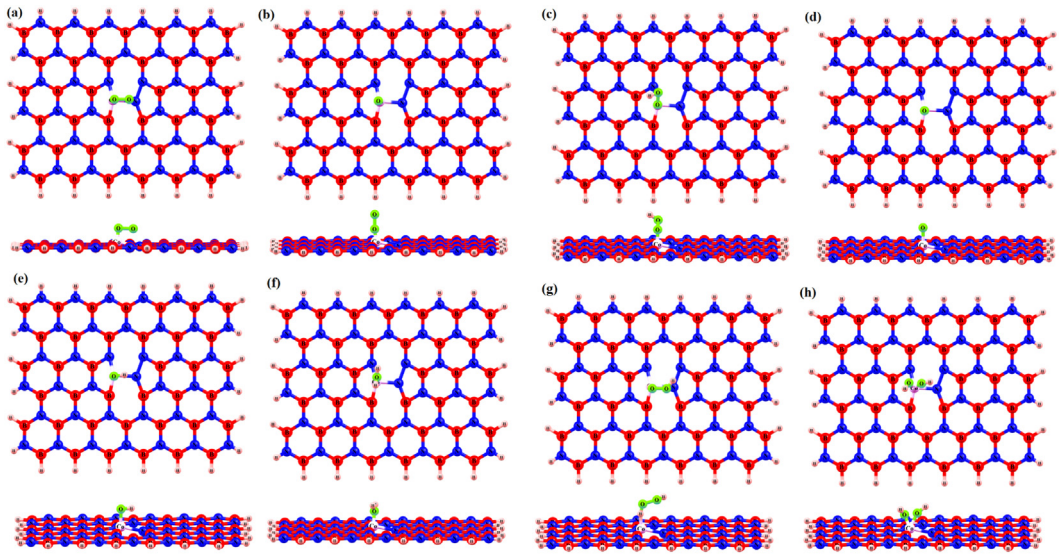

Fig. 3 – Atomic models of the adsorbed OCIs of Co-vacancy-BN monolayers (a,b) O_2*, (c) OOH*, (d) O*, (e) OH*, (f) HO_2*, (g) H_2O_2*, (h) OH*+OH*.

to the Co-adsorbed 2OH* or O*+H_2O* after H_2O_2 approaches Co atom. The O–Co distance was significantly less compared to that of others by 2.29 Å after H_2O_2 was adsorbed onto the raised side of Co-HBN, and it's the E_{ads} became larger by −1.03 eV. Thus, the formation of H_2O_2 was difficult to proceed.

3.3. *ORR progression*

The formation of the product H_2O_2 through adsorbed O_2* via the $2e^-$ reduction reaction route (RRR) or the product H_2O via the $4e^-$ RRR was possible. Clearly, the $4e^-$ RRR of O_2 was effective in the operation of PEMFCs. Based on the density functional theory estimations, the bond distance of O molecule in the gaseous phase was around 1.24 Å, but there was a stretching in the bond distance of O–O to around 1.31 Å following its adhesion onto the AC of Co–N. Numerous studies in the literature [45] have reported that the AC of Co–N can lead to a weakening in the O–O bond in the adsorbed O_2*, but it is not capable of promoting the dissociation of O_2* directly, which is why the dissociative activation energy for the dissociation of O_2 in the AC of CoN_4 is great large (reaching 1.94 eV) [46]. Hence, following the adhesion of O molecule onto the active site, the dissociation process proceeds the dissociation one. Hence, O_2* reduction into OOH* was the most suitable route for the ORRP. There was a further stretching in the O–O bond distance of OOH* adhesion geometry with most stability, and the O–O bond distance of OOH* adhered onto Co–N center increased 15.0% in comparison with O_2*. Despite the fact that there was a significant stretching in the O–O bond distance in OOH, the dissociation mechanism proceeds with difficulty. Nonetheless, its further hydrogenation was more facile to perform [45].

OOH could be hydrogenated for generating O* and H_2O, or could be directly reduced into H_2O_2* for further hydrogenation step. The O atom was farther from Co in OOH* in the second case, and it combined easily with proton ($H^+ + e^-$). At the same time, there was a cleavage in the O–O bond, which generated a H_2O molecule to escape from the catalytic surface and leave an oxygen atom that was still adsorbed onto the AC of Co–N. Next, the reduction of O* into OH * continued. Ultimately, it was reduced into H_2O via the last reduction process, which is in most cases is considered the rate-limiting step [47]. The direct generation of H_2O_2 for the latter case was difficult.

Table 1 – Adsorption energy (E_{ads}, eV) of the different ORR intermediates on Co-*vacancy*-BN, the corresponding Co–O bond distance (d, Å), charge-transfer (q, e) and atomic charge on the Co atom (q_a, |e|).

species	E_{ads} (eV)	d (Å)	q (e)	q_a (|e|)
O_2	−0.97	1.94	0.47	0.41
O	−3.89	1.73	0.60	0.39
OH	−2.69	1.86	0.30	0.34
OOH	−1.63	1.90	0.17	0.28
H_2O_2	−1.23	3.23	0.58	0.36
H_2O	−0.18	2.15	0.21	0.33

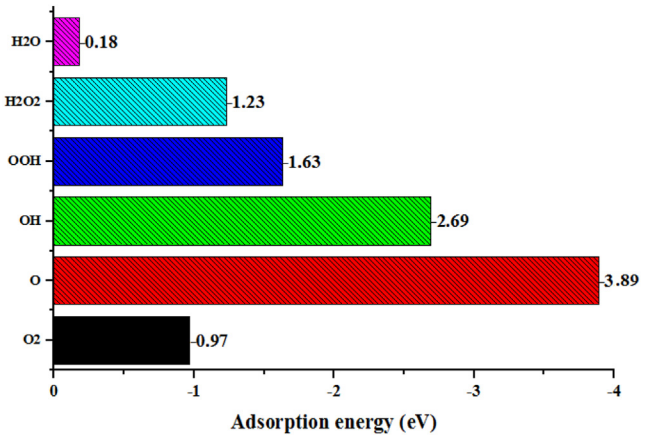

Fig. 4 – Adsorption energies of adsorbed OCIs on the Co–N active site.

Please cite this article as: Hsu C-Y et al., Design a promising electro-catalyst for oxygen reduction reaction in fuel cells based on transition metal doped in BN monolayer, International Journal of Hydrogen Energy, https://doi.org/10.1016/j.ijhydene.2023.08.085

Table 2 – Reaction free energies (eV) of the elementary reaction steps for Co-*vacancy*-BN.

Step	Free energies (eV)
$O_2+* \rightarrow O_2*$	−0.83
$O_2*+H^++e^- \rightarrow OOH*$	−0.70
$OOH*+H^++e^- \rightarrow O*+H_2O$	−1.43
$OOH*+H^++e^- \rightarrow H_2O_2+*$	−0.21
$OOH*+H^++e^- \rightarrow 2OH*$	−1.19
$2OH*+H^++e^- \rightarrow OH*+H_2O$	−1.98
$O*+H^++e^- \rightarrow OH*$	−1.56
$OH* + H^+ + e^- \rightarrow H_2O + *$	−0.57

We found that the adhesion of HOOH by these electrocatalysts was only possible at a long O–Co atomic distance. Furthermore, after HOOH approached the AC of Co–N, a decomposition of the O–O bond into the coadsorbed 2OH* or O + H_2O occurred. This demonstrated that after the generation of H_2O_2, it dissociated directly into 2 coadsorbed OH* or O* + H_2O* rather than the stabilization at H_2O_2, which depended upon the way H_2O_2 was located onto the surface of the electrocatalyst. We can consider this process a complete hydrogenation step (hydrogenation of OOH* in 2OH* or in H_2O*+ O*).

In connection with formation process of 2OH*, another OH* on the Co–N cluster could be further hydrogenated for forming H_2O, which leaves another OH* for the last reduction step. Furthermore, there was a possibility for the strong adhesion of H_2O_2 onto Co–N center of Co-HBN with a O–Co bond distance of 2.29 Å. The OOH* + H^+ + e^- → H_2O_2 + * reaction was exothermal, which indicated Co–N center was capable of promoting 2 e^- ORR for forming H_2O_2. In a study by Liu et al. it was found that the ORRP mainly proceeded in two-electron route on CoN_4 based on the experimental results (electron transport number was 2.5). Nonetheless, in a study by Li et al. it was found that [46] a 4e^- ORR was promoted on Co–N due to the instability of the H_2O_2 and its easy decomposition into 2 coadsorbed OH, whose stability was more than H_2O_2 in terms of energy. Based on the calculations, 2OH* was formed more easily than H_2O_2 on the Co– HBN. Additionally, based on the calculations, the hydrogenation of OOH* on Co doped Co-HBN was decomposed more easily into two 2OH* instead of forming H_2O_2. Based on the above-mentioned discussions, H_2O_2 was desorbed into the solution with difficulty during the ORR, and there were 2 possible routes for the 4e^- ORR.

Route 1: $O_2 \rightarrow O_2* \rightarrow OOH* \rightarrow O* \rightarrow OH* \rightarrow H_2O$

Route 2: $O_2 \rightarrow O_2* \rightarrow OOH* \rightarrow 2OH* \rightarrow OH* \rightarrow H_2O$

Table 1 provides the RFE for the process of O_2 reduction on these electrocatalysts. As shown in Table 1, the reaction energy for the hydrogenation of OH* for forming H_2O was the smallest, which was the rate-limiting step. Hence, in the presence of a non-zero electrode potential (U), the first reaction step that became endothermic thermodynamically (uphill) was the reduction of OH * into H_2O, which demonstrated under PEMFCs operating circumstances, the rate-limiting step for the ORRP on the AC of CoN_4 most apparently caused OH* to be reduced into H_2O. In case of route 2, there was a reduction of OOH* into 2OH* instead of O* + H_2O formation. It is possible to achieve the reaction route only for comparing the (RFE of OOH* + H^+ + e^- → O* + H_2O and OOH* + H^+ + e^- → 2OH* at the similar AC of Co–N. The ORRP proceeds in route 1 when the former is larger and the process proceeds in path II when the latter is larger. In the earlier sections, we determined the major ORR reaction routes on the different surfaces of electrocatalyst as well as the related changes in reaction free energy. It was found that the Co– HBN exhibited a promising activity for ORR reaction. In short, stability as well as ORR reactivity of these different electrocatalysts we evaluated. Co-doping made the Co-HBN electrocatalyst hump which was originally flat, which led to more activities on the AC of Co–N.

4. Conclusions

First-principles computations were undertaken to scrutinize the different reaction routes, reaction energies, and reaction barriers of the ORRP on Co-HBN. The results demonstrated that substituting B in HBN tended to capture the Co atom in comparison with substituting N. Based on the calculation of electronic properties, the AC for the ORR was the top site of Co. Moreover, the substantial difference of charge between N and Co on these electrocatalysts' surface suggested that the Co atom exhibited higher activity for adsorbing OCIs. In addition, there was a decrease in the E_{ads} for these OCIs in the order of O > OH > OOH > O_2 > H_2O_2 > H_2O over the surface of the electrocatalysts. Moreover, the larger energy of O_2 adhesion demonstrated that E_{ads} of OCIs was higher. Co-HBN electrocatalyst proceeded with the single Co site through the 4-electron ORRP via reaction route 2 (O2 → O2* → OOH* → 2OH* → OH* → H_2O). Additionally, the final reduction step ((OH* reduction) was the rate-limiting step for the ORRP over the electrocatalyst. The lower E_{ads} of OCIs suggested that the d-band center of Co was considerably distant from the FL, which demonstrated the more ORR activity as well as larger onset potential of the electrocatalyst.

Declaration of competing interest

The authors declare that they have no known competing financial interests or personal relationships that could have appeared to influence the work reported in this paper.

REFERENCES

[1] Wang W, Jia Q, Mukerjee S, Chen S. Recent insights into the oxygen-reduction electrocatalysis of Fe/N/C materials. ACS Catal 2019;9:10126–41.
[2] Liu H, Chen J, Hissel D, Lu J, Hou M, Shao Z. Prognostics methods and degradation indexes of proton exchange membrane fuel cells: a review. Renew Sustain Energy Rev 2020;123:109721.
[3] Chen X, Li C, Grätzel M, Kostecki R, Mao SS. Nanomaterials for renewable energy production and storage. Chem Soc Rev 2012;41:7909–37.
[4] Panwar N, Kaushik S, Kothari S. Role of renewable energy sources in environmental protection: a review. Renew Sustain Energy Rev 2011;15:1513–24.

Please cite this article as: Hsu C-Y et al., Design a promising electro-catalyst for oxygen reduction reaction in fuel cells based on transition metal doped in BN monolayer, International Journal of Hydrogen Energy, https://doi.org/10.1016/j.ijhydene.2023.08.085

[5] Gahleitner G. Hydrogen from renewable electricity: an international review of power-to-gas pilot plants for stationary applications. Int J Hydrogen Energy 2013;38:2039–61.
[6] Chen L, Xu X, Yang W, Jia J. Recent advances in carbon-based electrocatalysts for oxygen reduction reaction. Chin Chem Lett 2020;31:626–34.
[7] Dekel DR. Review of cell performance in anion exchange membrane fuel cells. J Power Sources 2018;375:158–69.
[8] Debe MK. Electrocatalyst approaches and challenges for automotive fuel cells. Nature 2012;486:43–51.
[9] Wang Y, Chen KS, Mishler J, Cho SC, Adroher XC. A review of polymer electrolyte membrane fuel cells: technology, applications, and needs on fundamental research. Appl Energy 2011;88:981–1007.
[10] Banham D, Ye S, Pei K, Ozaki J-i, Kishimoto T, Imashiro Y. A review of the stability and durability of non-precious metal catalysts for the oxygen reduction reaction in proton exchange membrane fuel cells. J Power Sources 2015;285:334–48.
[11] Xue Y, Sun S, Wang Q, Dong Z, Liu Z. Transition metal oxide-based oxygen reduction reaction electrocatalysts for energy conversion systems with aqueous electrolytes. J Mater Chem A 2018;6:10595–626.
[12] Wei D, Xue Z, Li L, Zi-dong W. Recent progress in heteroatoms doped carbon materials as a catalyst for oxygen reduction reaction. Journal of Electrochemistry 2014;20:426.
[13] Niu K, Yang B, Cui J, Jin J, Fu X, Zhao Q, Zhang J. Graphene-based non-noble-metal Co/N/C catalyst for oxygen reduction reaction in alkaline solution. J Power Sources 2013;243:65–71.
[14] Wang YC, Lai YJ, Song L, Zhou ZY, Liu JG, Wang Q, Yang XD, Chen C, Shi W, Zheng YP. S-doping of an Fe/N/C ORR catalyst for polymer electrolyte membrane fuel cells with high power density. Angew Chem 2015;127:10045–8.
[15] Rojas-Carbonell S, Santoro C, Serov A, Atanassov P. Transition metal-nitrogen-carbon catalysts for oxygen reduction reaction in neutral electrolyte. Electrochem Commun 2017;75:38–42.
[16] Liu B, Huang B, Lin C, Ye J, Ouyang L. Porous carbon supported Fe-NC composite as an efficient electrocatalyst for oxygen reduction reaction in alkaline and acidic media. Appl Surf Sci 2017;411:487–93.
[17] Jiang S, Zhu C, Dong S. Cobalt and nitrogen-cofunctionalized graphene as a durable non-precious metal catalyst with enhanced ORR activity. J Mater Chem A 2013;1:3593–9.
[18] Yin P, Yao T, Wu Y, Zheng L, Lin Y, Liu W, Ju H, Zhu J, Hong X, Deng Z. Single cobalt atoms with precise N-coordination as superior oxygen reduction reaction catalysts. Angew Chem 2016;128:10958–63.
[19] Zhao S, Yang J, Han M, Wang X, Lin Y, Yang R, Xu D, Shi N, Wang Q, Yang M. Synergistically enhanced oxygen reduction electrocatalysis by atomically dispersed and nanoscaled Co species in three-dimensional mesoporous Co, N-codoped carbon nanosheets network. Appl Catal B Environ 2020;260:118207.
[20] Yang Z, Nie H, Chen X, Huang S. Recent progress in doped carbon nanomaterials as effective cathode catalysts for fuel cell oxygen reduction reaction. J Power Sources 2013;236:238–49.
[21] Zhu C, Dong S. Recent progress in graphene-based nanomaterials as advanced electrocatalysts towards oxygen reduction reaction. Nanoscale 2013;5:1753–67.
[22] Daems N, Sheng X, Vankelecom IF, Pescarmona PP. Metal-free doped carbon materials as electrocatalysts for the oxygen reduction reaction. J Mater Chem A 2014;2:4085–110.
[23] Zhou M, Wang H-L, Guo S. Towards high-efficiency nanoelectrocatalysts for oxygen reduction through engineering advanced carbon nanomaterials. Chem Soc Rev 2016;45:1273–307.
[24] Weng Q, Wang X, Wang X, Bando Y, Golberg D. Functionalized hexagonal boron nitride nanomaterials: emerging properties and applications. Chem Soc Rev 2016;45:3989–4012.
[25] Zhang K, Feng Y, Wang F, Yang Z, Wang J. Two dimensional hexagonal boron nitride (2D-hBN): synthesis, properties and applications. J Mater Chem C 2017;5:11992–2022.
[26] Zheng Z, Cox M, Li B. Surface modification of hexagonal boron nitride nanomaterials: a review. J Mater Sci 2018;53:66–99.
[27] Kim G, Jang A-R, Jeong HY, Lee Z, Kang DJ, Shin HS. Growth of high-crystalline, single-layer hexagonal boron nitride on recyclable platinum foil. Nano Lett 2013;13:1834–9.
[28] Wang J, Ma F, Sun M. Graphene, hexagonal boron nitride, and their heterostructures: properties and applications. RSC Adv 2017;7:16801–22.
[29] Meng J, Wang D, Cheng L, Gao M, Zhang X. Recent progress in synthesis, properties, and applications of hexagonal boron nitride-based heterostructures. Nanotechnology 2018;30:074003.
[30] Han W-Q, Brutchey R, Tilley TD, Zettl A. Activated boron nitride derived from activated carbon. Nano Lett 2004;4:173–6.
[31] Meng X-L, Lun N, Qi Y-X, Zhu H-L, Han F-D, Yin L-W, Fan R-H, Bai Y-J, Bi J-Q. Simple synthesis of mesoporous boron nitride with strong cathodoluminescence emission. J Solid State Chem 2011;184:859–62.
[32] Zhang X, Lian G, Si H, Wang J, Cui D, Wang Q. Novel BN porous-hollow nanorods: synthesis, tunable dimensions, property and formation mechanism. J Mater Chem A 2013;1:11992–8.
[33] Lei W, Portehault D, Liu D, Qin S, Chen Y. Porous boron nitride nanosheets for effective water cleaning. Nat Commun 2013;4:1–7.
[34] Kattel S, Atanassov P, Kiefer B. Catalytic activity of Co–N x/C electrocatalysts for oxygen reduction reaction: a density functional theory study. Phys Chem Chem Phys 2013;15:148–53.
[35] Zhu G, Liu F, Wang Y, Wei Z, Wang W. Systematic exploration of N, C coordination effects on the ORR performance of Mn–N x doped graphene catalysts based on DFT calculations. Phys Chem Chem Phys 2019;21:12826–36.
[36] Olson TS, Pylypenko S, Atanassov P, Asazawa K, Yamada K, Tanaka H. Anion-exchange membrane fuel cells: dual-site mechanism of oxygen reduction reaction in alkaline media on cobalt– polypyrrole electrocatalysts. J Phys Chem C 2010;114:5049–59.
[37] Schmidt MW, Baldridge KK, Boatz JA, Elbert ST, Gordon MS, Jensen JH, Koseki S, Matsunaga N, Nguyen KA, Su S, Windus TL, Dupuis M, Montgomery JA. General atomic and molecular electronic structure system. J Comput Chem 1993;14:1347–63.
[38] Grimme S. Semiempirical GGA-type density functional constructed with a long-range dispersion correction. J Comput Chem 2006;27:1787–99.
[39] Shang Y, Zhao J-x, Wu H, Cai Q-h, Wang X-g, Wang X-z. Chemical functionalization of pyridine-like and porphyrin-like nitrogen-doped carbon (CN x) nanotubes with transition metal (TM) atoms: a theoretical study. Theor Chem Acc 2010;127:727–33.
[40] Nørskov JK, Rossmeisl J, Logadottir A, Lindqvist L, Kitchin JR, Bligaard T, Jonsson H. Origin of the overpotential for oxygen reduction at a fuel-cell cathode. J Phys Chem B 2004;108:17886–92.
[41] Li L, Yu X, Yang X, Fang Y, Zhang X, Xu X, Jin P, Tang C. Porous BN with vacancy defects for selective removal of CO

Please cite this article as: Hsu C-Y et al., Design a promising electro-catalyst for oxygen reduction reaction in fuel cells based on transition metal doped in BN monolayer, International Journal of Hydrogen Energy, https://doi.org/10.1016/j.ijhydene.2023.08.085

from H 2 feed gas in hydrogen fuel cells: a DFT study. J Mater Chem A 2016;4:15631–7.
[42] Zhang H, Tong C-J, Zhang Y, Zhang Y-N, Liu L-M. Porous BN for hydrogen generation and storage. J Mater Chem A 2015;3:9632–7.
[43] Zhao J-x, Wang H-x, Liu Y-j, Cai Q-h, Wang X-z. Catalyst-free achieving of controllable carbon doping of boron nitride nanosheets by CO molecules: a theoretical prediction. RSC Adv 2013;3:4917–26.
[44] Li Q, Zhang T, Yu X, Wu X, Zhang X, Lu Z, Yang X, Huang Y, Li L. Isolated Au atom anchored on porous boron nitride as a promising electrocatalyst for oxygen reduction reaction (ORR): a DFT study. Front Chem 2019;7:674.
[45] Zhang X, Lu Z, Yang Z. The mechanism of oxygen reduction reaction on CoN4 embedded graphene: a combined kinetic and atomistic thermodynamic study. Int J Hydrogen Energy 2016;41:21212–20.
[46] Li F, Shu H, Hu C, Shi Z, Liu X, Liang P, Chen X. Atomic mechanism of electrocatalytically active Co–N complexes in graphene basal plane for oxygen reduction reaction. ACS Appl Mater Interfaces 2015;7:27405–13.
[47] Wang XX, Cullen DA, Pan YT, Hwang S, Wang M, Feng Z, Wang J, Engelhard MH, Zhang H, He Y. Nitrogen-coordinated single cobalt atom catalysts for oxygen reduction in proton exchange membrane fuel cells. Adv Mater 2018;30:1706758.

Please cite this article as: Hsu C-Y et al., Design a promising electro-catalyst for oxygen reduction reaction in fuel cells based on transition metal doped in BN monolayer, International Journal of Hydrogen Energy, https://doi.org/10.1016/j.ijhydene.2023.08.085